Effect of multiple conduction bands on high-harmonic emission from dielectrics

Peter G. Hawkins,[1,*] Misha Yu. Ivanov,[1,2] and Vladislav S. Yakovlev[3,4,5]

[1]*Department of Physics, Imperial College London, South Kensington Campus, SW7 2AZ London, United Kingdom*

[2]*Max-Born-Institute, Max-Born Strasse 2A, D-12489 Berlin, Germany*

[3]*Max-Planck-Institut für Quantenoptik, Hans-Kopfermann-Straße 1, D-85748 Garching, Germany*

[4]*Department für Physik der Ludwig-Maximilians-Universität München, Am Coulombwall 1, D-58748 Garching, Germany*

[5]*Center for Nano-Optics, Department of Physics and Astronomy, Georgia State University, Atlanta, Georgia 30303, USA*

(Received 9 May 2014; revised manuscript received 30 September 2014; published 14 January 2015)

We find that, for sufficiently strong mid-IR fields, transitions between different conduction bands play an important role in the generation of high-order harmonics in a dielectric. The transitions make a significant contribution to the harmonic signal, and they can create a single effective band for the motion of an electron wave packet. We show how high harmonic spectra produced during the interaction of ultrashort laser pulses with periodic solids provide a spectroscopic tool for understanding the effective band structure that controls electron dynamics in these media.

DOI: 10.1103/PhysRevA.91.013405 PACS number(s): 32.80.Rm, 42.50.Hz, 42.65.Ky, 78.47.J−

High-order harmonic generation (HHG) from gas targets is now used as a spectroscopic tool for imaging nuclear (see, e.g., [1–3]) and electronic (see, e.g., [4–7]) dynamics on the atomic time and length scales. It is sensitive to various aspects of electronic dynamics, from attosecond processes in neutral systems [8,9] to hole dynamics in ions [4–7], correlation-driven channel interaction [10–12], and time- and space-resolved information on electronic transitions from different molecular orbitals [13–15].

We show that HHG spectra from periodic solids give insight into the effective band structure established by a strong driving mid-infrared laser field. Pioneering experiments on high harmonic generation from dielectrics [16,17] stimulated a simple model offering semiclassical insight into the underlying physics. In this model ([16,18]; see also [19]) electrons first tunnel from a valence band (VB) to a conduction band (CB) at the maxima of the electric field. There, they are driven along the single conduction band by the field. The harmonic intensity at frequency ω is then given by $|\omega J(\omega)|^2$, where $J(\omega)$ is the Fourier transform of the current, $j(t)$, in the conduction band $\varepsilon(k)$. Since in this model $j(t) \propto v(t) \propto d\varepsilon/dk$, where $v(t)$ is the electron group velocity, analysis of the harmonic spectrum can yield information about the band structure $(d\varepsilon/dk)$. This picture predicts that, when the driving mid-IR laser is sufficiently strong to rapidly accelerate electrons to the edge of the Brillouin zone (BZ), Bragg reflections (Bloch oscillations) within the single band would generate most of the high harmonics.

However, if electrons quickly move past the gap between adjacent CBs, they may undergo an interband transition. In this case, the harmonic signal also comes from coherences between all participating bands, including the VB [17,20]. Additionally it is also important to account for the temporal structure of all interband transitions, including the VB to CB transition; see, e.g., [21]. Recent theoretical analysis of HHG in bulk solids by Vampa *et al.* [22] and Higuchi *et al.* [23] accounted for the temporal structure of interband excitations, but as two-band models were used in both cases, transitions between conduction bands were not considered. We note that early work by Plaja *et al.* [24] did consider multiple bands.

We show that the inclusion of multiple conduction bands leads to additional contributions to the high-harmonic signal and that, in spite of the increasing complexity, the essential information about the motion of electrons in multiple conduction bands is contained in harmonic spectra. In particular, it reflects the formation of a single, effective CB due to the efficient inter-CB transitions for sufficiently strong driving fields.

We solve the time-dependent Schrödinger equation (TDSE) for an electron in a periodic potential:

$$\hat{H}\Psi(\boldsymbol{r},t) = \left[\frac{[\boldsymbol{p}+\boldsymbol{A}(t)]^2}{2} + U(\boldsymbol{r})\right]\Psi = i\frac{\partial\Psi}{\partial t}, \qquad (1)$$

where $\boldsymbol{A}(t)$ is the vector potential of the electric field $\boldsymbol{F}(t) = -\boldsymbol{A}'(t)$, and $U(\boldsymbol{r})$ is the periodic potential of the crystal. In (1) and below atomic units are used. We write $\Psi(\boldsymbol{r},t)$ for an initial crystal momentum $\boldsymbol{k}_0$ as

$$\left|\Psi_{\boldsymbol{k}_0}(t)\right\rangle = \sum_n \alpha^n_{\boldsymbol{k}_0}(t) e^{-i\int^t \epsilon^n_{\boldsymbol{k}(t')}dt'} e^{-i\boldsymbol{A}(t)\boldsymbol{r}} \left|\phi^n_{\boldsymbol{k}(t)}\right\rangle, \qquad (2)$$

where $|\phi^n_{\boldsymbol{k}(t)}\rangle$ and $\epsilon^n_{\boldsymbol{k}(t)}$ are the Bloch states and associated energies of the field-free system, with the time dependence of the crystal momentum being $\boldsymbol{k}(t) = \boldsymbol{k}_0 + \boldsymbol{A}(t)$. The index n labels the band of the state, and $\boldsymbol{k}_0$ parametrizes the drift momentum. Note that $e^{-i\boldsymbol{A}(t)\boldsymbol{r}}|\phi^n_{\boldsymbol{k}(t)}\rangle$ are known as Houston states; see, e.g., [25]. We use the so-called periodic gauge [26]: $|\phi^n_{\boldsymbol{k}+\boldsymbol{G}}\rangle = |\phi^n_{\boldsymbol{k}}\rangle$, where $\boldsymbol{G}$ is a vector of the reciprocal lattice. That is, whenever $\boldsymbol{k}(t)$ lies outside of the first BZ, the periodicity of wave functions with respect to the crystal momentum is assumed.

Our main focus is the modification of the band structure in strong fields, thus we study the single particle response. Substituting the ansatz (2) into Eq. (1) yields the set of coupled differential equations for $\alpha^n_{\boldsymbol{k}_0}(t)$:

$$\frac{d}{dt}\alpha^n_{\boldsymbol{k}_0}(t) = -i\boldsymbol{F}(t)\sum_{n'}\boldsymbol{\xi}^{n,n'}_{\boldsymbol{k}(t)}\alpha^{n'}_{\boldsymbol{k}_0}(t)e^{i\int^t \Delta\varepsilon^{n,n'}_{\boldsymbol{k}(t')}dt'}. \qquad (3)$$

*peter.hawkins08@imperial.ac.uk

Here, $\Delta\varepsilon^{n,n'}_{\boldsymbol{k}(t)} = \varepsilon^{n}_{\boldsymbol{k}(t)} - \varepsilon^{n'}_{\boldsymbol{k}(t)}$, and $\boldsymbol{\xi}^{n,n'}_{\boldsymbol{k}(t)}$ is given by

$$\boldsymbol{\xi}^{n,n'}_{\boldsymbol{k}(t)} = i\left\langle \nu^{n}_{\boldsymbol{k}(t)} \middle| \nabla_{\boldsymbol{k}} \middle| \nu^{n'}_{\boldsymbol{k}(t)} \right\rangle, \tag{4}$$

where ν is the lattice-periodic part of the Bloch state: $\langle \boldsymbol{r}|\phi^{n}_{\boldsymbol{k}}\rangle = \nu^{n}_{\boldsymbol{k}}(\boldsymbol{r})\exp(i\boldsymbol{k}\boldsymbol{r})$.

We use the initial condition that the VBs are fully populated across the whole BZ before the interaction with the laser pulse, with the CBs being unoccupied. That is, we solve the TDSE independently for each pair of $n \in$ VB and $\boldsymbol{k}_0$.

After finding $\Psi_{\boldsymbol{k}_0}(t)$, we obtain the contributions to the current at a particular $\boldsymbol{k}_0$: $\boldsymbol{j}_{\boldsymbol{k}_0} = \langle \Psi_{\boldsymbol{k}_0}|\hat{\boldsymbol{p}} + \boldsymbol{A}(t)|\Psi_{\boldsymbol{k}_0}\rangle$, which is then integrated over the BZ to obtain the full current averaged over the unit cell:

$$\boldsymbol{j}(t) = \int_{\mathrm{BZ}} \boldsymbol{j}_{\boldsymbol{k}_0}(t) d^3\boldsymbol{k}_0, \tag{5}$$

$$\boldsymbol{j}_{\boldsymbol{k}_0}(t) = \sum_{n,n'} \boldsymbol{a}^{n,n'}_{\boldsymbol{k}_0}(t) \exp\left(i\int^{t} \Delta\varepsilon^{n,n'}_{\boldsymbol{k}(t')} dt' \right), \tag{6}$$

$$\boldsymbol{a}^{n,n'}_{\boldsymbol{k}_0}(t) = \left(\alpha^{n}_{\boldsymbol{k}_0}(t)\right)^{*} \alpha^{n'}_{\boldsymbol{k}_0}(t) \boldsymbol{p}^{n,n'}_{\boldsymbol{k}(t)}. \tag{7}$$

Here $\boldsymbol{p}^{n,n'}_{\boldsymbol{k}(t)}$ are the momentum matrix elements between Bloch states: $\langle \phi^{n}_{\boldsymbol{k}(t)}|\hat{\boldsymbol{p}}|\phi^{n'}_{\boldsymbol{k}(t)}\rangle$.

Three distinct physical effects contributing to the generation of high-frequency components can be identified in the electric current. First, the group velocity, which is equal to the mean momentum $\boldsymbol{p}^{n,n}_{\boldsymbol{k}(t)}$, changes its sign as an electron crosses a boundary of the BZ remaining in the same band, in which case it experiences a Bragg reflection. This causes a rapid change of the intraband current, which is the part of Eq. (6) with $n = n'$:

$$\boldsymbol{j}^{(\mathrm{intraband})}_{\boldsymbol{k}_0}(t) = \sum_{n} \left|\alpha^{n}_{\boldsymbol{k}_0}(t)\right|^2 \boldsymbol{p}^{n,n}_{\boldsymbol{k}(t)}. \tag{8}$$

Such Bragg reflections are believed to be the main mechanism responsible for the observed HHG [17,18,23]. Second, the coherent superposition of any two states with an allowed dipole transition results in quantum beats. This contribution was analyzed in [22], where it was pointed out that dephasing strongly suppresses the quantum-beat signal, which is dominant otherwise. Finally, transitions between conduction bands that occur in the regions where gaps are small can also lead to a very rapid change in the terms associated with interband coherences ($n \neq n'$), provided that $p^{n,n_0}_{\tilde{\boldsymbol{k}}} \neq p^{n',n_0}_{\tilde{\boldsymbol{k}}}$, where n_0 is the index of the electron's initial (valence) band, and $\tilde{\boldsymbol{k}}$ is a crystal momentum where the gap between bands n and n' is minimal. This last contribution has not yet been studied.

To obtain an explicit expression for the part of $\boldsymbol{j}_{\boldsymbol{k}_0}(t)$ that arises as an immediate effect of the external field, we differentiate Eq. (6) with time:

$$\frac{d}{dt}\boldsymbol{j}_{\boldsymbol{k}_0}(t) = \frac{d}{dt}\boldsymbol{j}^{(\mathrm{tr})}_{\boldsymbol{k}_0}(t) + \frac{d}{dt}\boldsymbol{j}^{(\mathrm{QB})}_{\boldsymbol{k}_0}(t), \tag{9}$$

$$\frac{d}{dt}\boldsymbol{j}^{(\mathrm{tr})}_{\boldsymbol{k}_0}(t) = \sum_{n,n'} e^{i\int^{t}\Delta\varepsilon^{n,n'}_{\boldsymbol{k}(t')}dt'} \frac{d}{dt}\boldsymbol{a}^{n,n'}_{\boldsymbol{k}_0}(t), \tag{10}$$

$$\frac{d}{dt}\boldsymbol{j}^{(\mathrm{QB})}_{\boldsymbol{k}_0}(t) = i\sum_{n,n'} \Delta\varepsilon^{n,n'}_{\boldsymbol{k}(t)} e^{i\int^{t}\Delta\varepsilon^{n,n'}_{\boldsymbol{k}(t')}dt'} \boldsymbol{a}^{n,n'}_{\boldsymbol{k}_0}(t). \tag{11}$$

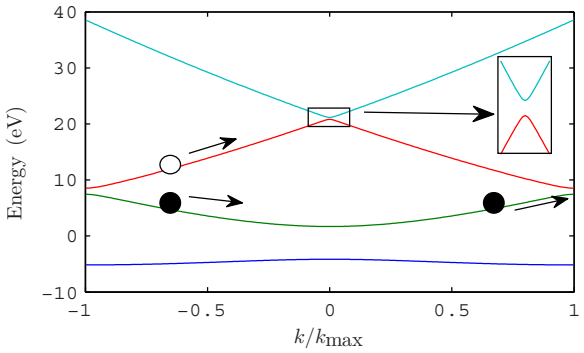

FIG. 1. (Color online) The upper valence band and first three conduction bands used in the simulations. Electrons reaching the Bragg plane can stay in the same band, reflecting, shown here as the circle remaining black. Alternatively they can undergo a transition to the next CB, white circle.

In our model, which does not explicitly account for dephasing, the quantum-beat current $\boldsymbol{j}^{(\mathrm{QB})}_{\boldsymbol{k}_0}(t)$ gradually grows as the concentration of charge carriers increases, and it persists after the laser pulse. In contrast, the derivative of the *transient current* $\boldsymbol{j}^{(\mathrm{tr})}_{\boldsymbol{k}_0}(t)$ becomes zero as soon as the external field disappears, and it is affected by any rapid change of matrix elements or probability amplitudes that may occur at an avoided crossing between bands. In the following, we will focus on $\boldsymbol{j}^{(\mathrm{tr})}_{\boldsymbol{k}_0}(t)$, assuming that the contribution from $\boldsymbol{j}^{(\mathrm{QB})}_{\boldsymbol{k}_0}(t)$ to sufficiently high frequencies is suppressed by dephasing phenomena. This division of the current density into two different parts is different from the division in the interband and intraband currents in [17,22], while the intraband current is fully included in $\boldsymbol{j}^{(\mathrm{tr})}_{\boldsymbol{k}_0}(t)$. The proposed separation of the currents has the drawback that neither $\boldsymbol{j}^{(\mathrm{tr})}_{\boldsymbol{k}_0}(t)$ nor $\boldsymbol{j}^{(\mathrm{QB})}_{\boldsymbol{k}_0}(t)$ alone account for the linear polarization response, but, as we show below, it is very useful to analyze and visualize the high-frequency response.

To simplify our simulations and the subsequent analysis, we solve the TDSE problem in one spatial dimension. We obtain the energies and matrix elements by solving the stationary Schrödinger equation for a periodic lattice potential $U(x)$ that, within the central unit cell, has the following form: $U(x) = -U_0[1 + \tanh(x + x_0)][1 + \tanh(-x + x_0)]$. This potential allows us to reproduce the key parameter of a real solid: the band gap. Setting our parameters to $U_0 = 0.78$, $x_0 = 0.565$, with lattice spacing $a = 8.15$ a.u. yields a VB-CB band gap of 5.85 eV; the band gap and lattice constant mimic the structure of AlN. The gaps between the conduction bands are smaller, with the first CB gap being 1.09 eV. The highest VB and first three CBs are shown in Fig. 1, plotted as a function of $k/k_{\max}$ with $k_{\max} = \pi/a$.

We consider laser pulses at $\lambda_{\mathrm{L}} = 1800\,\mathrm{nm}$ ($\omega_{\mathrm{L}} = 2\pi c/\lambda_{\mathrm{L}} = 1.05\,\mathrm{fs}^{-1}$), with a field strength of 0.75 $\mathrm{V\AA}^{-1}$, and a full width half maximum (FWHM) of 30 fs. The envelope used for the vector potential is of the following form: $\cos^4(\pi t/2\tau)$, where $\tau = (\pi/4)[\tau_{\mathrm{FWHM}}/\cos^{-1}(2^{-0.125})]$.

To highlight the importance of multiple conduction bands, as well as the interplay of Bragg reflections and transitions between conduction bands, in Fig. 2 we show the intraband

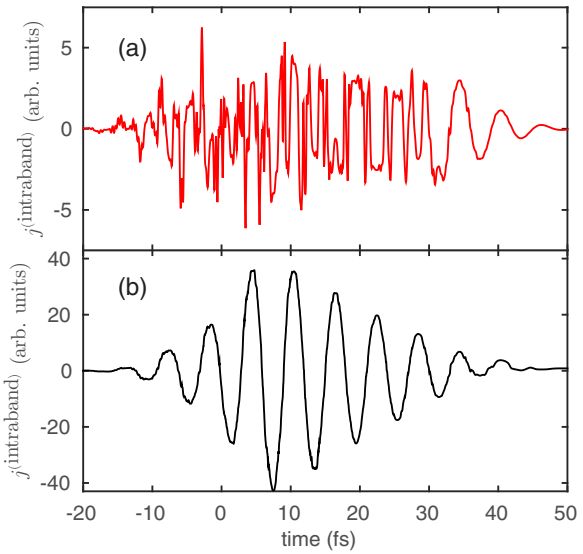

FIG. 2. (Color online) (a) Shows the intraband current with only one CB; in this case interband transition to higher CBs cannot happen and so Bragg reflections are forced to occur, explaining the appearance of higher harmonic content. (b) Shows the intraband current for eight CBs.

current. For a single CB, the intraband current shows strong Bragg reflections and Bloch oscillations, Fig. 2(a). However, as soon as multiple bands are included, these effects disappear and the intraband current is dominated by the fundamental frequency, Fig. 2(b). In the absence of reflections, electrons would move on an almost parabolic potential. This motion would result in a current composed almost entirely of the fundamental frequency. The fact that including more than a single CB leads to a large increase of the fundamental relative to higher harmonics suggests that transitions between CBs dominate the effect of Bragg reflections. That is, electrons move on a single effective nearly parabolic potential due to the dressing of the system by the strong laser field. Clearly, for such fields a simulation with a single CB is inadequate; we used eight CBs as this is the requirement for convergence.

This effect is easily visualized by plotting $|\alpha^n_{\boldsymbol{k}_0}(t)|^2$ for conduction bands in the extended zone scheme, as can be seen in Fig. 3. As electrons pass by BZ edges the most probable path

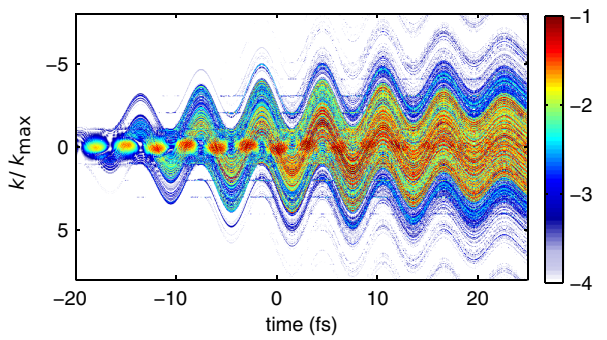

FIG. 3. (Color online) The time-dependent conduction band population is plotted on a logarithmic scale in the extended zone scheme, so that the n$^{\mathrm{th}}$ CB occupies crystal momenta $n-1 < |k|/k_{\mathrm{max}} < n$. The high transition probability between CBs is easily seen.

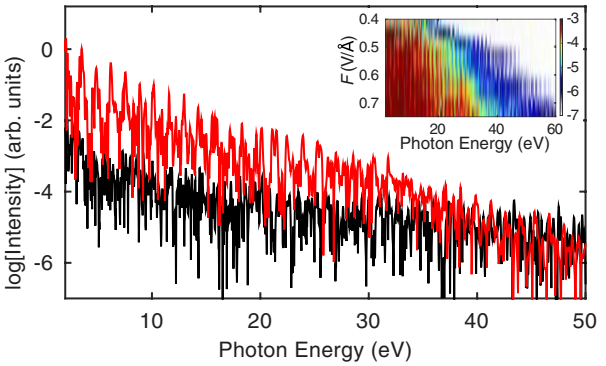

FIG. 4. (Color online) The harmonic spectrum generated by the transient current is plotted for the single- (red, upper line) and many-CB (black) cases. The variation of the spectra with field strength is shown in the inset plot for the single CB case.

changes from Bragg reflection early in the pulse into transition into the higher CBs as the IR intensity grows.

We now focus on the transient current (10). In Fig. 4 the spectrum of the transient current is shown for the many and single CB cases. The harmonic content is much more defined for the single CB case. The inset in Fig. 4 is the field dependence of the spectra for the single CB case, in a similar style of plotting to that used in [23]. The cutoff scaling is seen to be linear with field strength as in experiments [16,17]. Note that for the multiple CB case with the band structure used here, transitions saturate quickly leading to a breakdown of the cutoff scaling.

We note here that the harmonics in both spectra in Fig. 4 are poorly resolved, especially in the case of many conduction bands. The work of Vampa *et al.* [22] explains that the absence of dephasing in the model will lead to poorly defined harmonics. However, the lack of dephasing in our model does not prevent us from showing how the presence of multiple CBs affects the harmonic spectra in several fundamental and possibly observable ways.

To understand the time dependence of the harmonic emission we employ time-frequency analysis of the transient current obtained via the Morlet wavelet transform:

$$W(\Omega,\tau) = \int dt\, j^{(\mathrm{tr})}(t) e^{i\Omega t} e^{-\left(\frac{\Omega(t-\tau)}{\sqrt{2}\sigma\Omega_c}\right)^2}, \qquad (12)$$

where σ is selected to yield 14% of a cycle width at $\Omega_c = 15\omega_{\mathrm{L}}$. The width of the time-domain window then decreases with increasing Ω, improving the resolution.

The result is plotted in Fig. 5. For the single CB case, emission is half-cycle periodic, with bursts around the peaks of the electric field. This is particularly true for photon energies above the maximal bandgap between the upper VB and lower CB. Indeed, this is when the electrons experience highest acceleration past the BZ edge, thus generating the highest harmonic content when Bragg reflected in the single-CB model. However, when multiple CBs are included the bursts of emission are not so well defined temporally. We also see that the most intense harmonic emission occurs after the center of the pulse in both cases. This is because the concentration of charge carriers continues to grow after the peak of the pulse, which compensates for the decrease of the field.

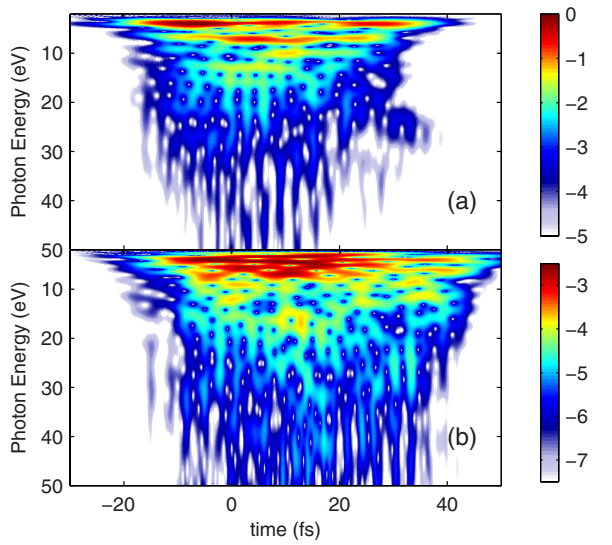

FIG. 5. (Color online) Time-frequency analysis, as described in the text, of the transient current for the single- (a) and many- (b) CB cases is plotted. One can immediately see that the emission for the single-CB case is occurring in bursts that are more defined than in the many-CB case.

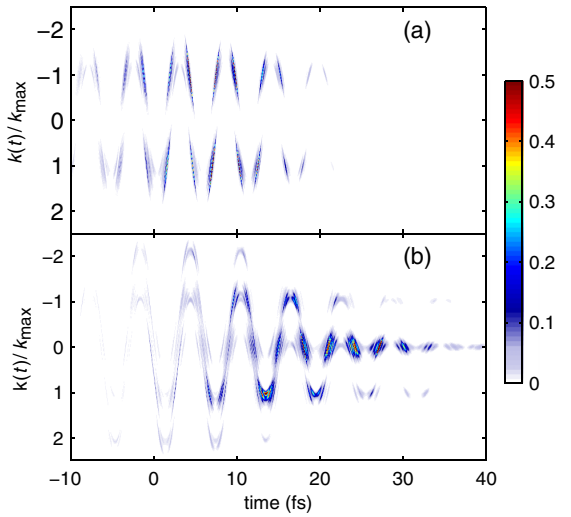

FIG. 6. (Color online) The strength of the harmonic emission given by the transient current, when multiplied with a Gaussian window centered around 30 eV and FWHM of 5 eV, is plotted as a function of the time-dependent crystal momentum and time for the single- (a) and many- (b) CB cases. For the single-CB case we see the emission is occurring at the Bragg planes: $|k| = k_{\max}$. For the many-CB case a lot of the emission is at $k = 0$, particularly at larger times.

To see where in the band structure and at what times in the field harmonic emission occurs, we develop another technique. The harmonic spectrum generated by electrons with initial crystal momentum $\boldsymbol{k}_0$ is given by the Fourier transform of $\boldsymbol{j}^{(\mathrm{tr})}_{\boldsymbol{k}_0}(t)$. We take the product of a Gaussian window with the harmonic spectrum for a given $\boldsymbol{k}_0$ to select a spectral region of interest:

$$J^{(\mathrm{tr})}_{\boldsymbol{k}_0}(\omega;\omega_0,\sigma) = \mathcal{F}\big[\boldsymbol{j}^{(\mathrm{tr})}_{\boldsymbol{k}_0}(t)\big]\exp\left(-\frac{(\omega-\omega_0)^2}{2\sigma^2}\right). \qquad (13)$$

This allows us to investigate the temporal profile of emission in this spectral region: For a given $\boldsymbol{k}_0$, the envelope of harmonic bursts is thus given by $E(t,\boldsymbol{k}_0;\omega_0,\sigma) = \mathcal{F}^{-1}[J^{\mathrm{tr}}_{\boldsymbol{k}_0}]$. Since every $\boldsymbol{k}_0$ is related to $\boldsymbol{k}(t)$, it also allows us to map the harmonic emission in the spectral region to the time at which it occurs, and the crystal momentum at that time.

In Fig. 6 this analysis is applied to compare the nature of the harmonic emission in the single- and many-CB cases. It allows us to clearly see that for the single-CB case the harmonic emission is dominated by electrons reflected at Bragg planes. For the many-CB case the process is modified; we still see that there is some emission around the Bragg plane from electrons reflecting at and crossing it. At later times there is emission for electrons with crystal momentum of $k = 0$; this acts to prolong the time over which emission occurs compared to the single-CB case. We attribute the prolonged emission at $k = 0$ to be due to electrons crossing between the second and third CBs, where the gap is small (see Fig. 1) so that even at reduced field the transition probability is still large.

It was observed in experiments that HHG in a crystalline solid is particularly efficient for certain orientations of the sample with respect to the polarization of the fundamental field [16,17]. Our results suggest that the observed angular dependence is mainly due to transitions between CBs, which occur at local minima of inter-CB energy gaps, and the probability of which is very sensitive to the magnitudes of the gaps.

Our most important finding is that such interband transitions not only reduce the intensity of harmonic emission, but they can also have a strong impact on its spectral and temporal properties: Individual harmonics become less distinct, and the rapid change of the quantum-beat signal associated with interband transitions plays a particularly important role in higher CBs. To study these effects, we have identified a useful quantity, the transient current, that allows the nature of the harmonic emission to be disentangled from quantum beats that are expected to be strongly suppressed by dephasing in real solids. The relative importance of Bragg reflections and interband transitions is sensitive to the band structure and field parameters, but the statement that Zener-like transitions between conduction bands result in the emission of high-frequency radiation is general. This effect may be used to experimentally study the motion of electrons driven by a strong mid-IR field in an effective single nearly parabolic band, once temporal characterization of harmonics emitted from a solid sample becomes feasible.

P.H. and M.I. were supported by EPSRC programme Grant No. EP/I032517/1; they also acknowledge support from Marie Curie ITN CORINF. V.S.Y. was supported by the DFG Cluster of Excellence, Munich-Centre for Advanced Photonics (MAP). He is grateful to S. Kruchinin, E. Goulielmakis, and M. Stockman for useful discussions. This work was (partially) supported by the U.S. Air Force Office of Scientific Research under Program No. FA9550-12-1-0482.

[1] S. Baker, J. S. Robinson, C. Haworth, H. Teng, R. Smith, C. Chirilă, M. Lein, J. Tisch, and J. Marangos, Science **312**, 424 (2006).
[2] M. Lein, J. Phys. B **40**, R135 (2007).
[3] H. J. Worner, J. B. Bertrand, D. V. Kartashov, P. B. Corkum, and D. M. Villeneuve, Nature (London) **466**, 604 (2010).
[4] O. Smirnova, Y. Mairesse, S. Patchkovskii, N. Dudovich, D. Villeneuve, P. Corkum, and M. Y. Ivanov, Nature (London) **460**, 972 (2009).
[5] S. Haessler, J. Caillat, W. Boutu, C. Giovanetti-Teixeira, T. Ruchon, T. Auguste, Z. Diveki, P. Breger, A. Maquet, B. Carre, R. Taieb, and P. Salieres, Nature Phys. **6**, 200 (2010).
[6] O. Smirnova, S. Patchkovskii, Y. Mairesse, N. Dudovich, and M. Y. Ivanov, Proc. Nat. Acad. Sci. USA **106**, 16556 (2009).
[7] Y. Mairesse, J. Higuet, N. Dudovich, D. Shafir, B. Fabre, E. Mével, E. Constant, S. Patchkovskii, Z. Walters, M. Y. Ivanov, and O. Smirnova, Phys. Rev. Lett. **104**, 213601 (2010).
[8] V. Averbukh, Phys. Rev. A **69**, 043406 (2004).
[9] H. Niikura, D. M. Villeneuve, and P. B. Corkum, Phys. Rev. Lett **94**, 083003 (2005).
[10] S. Sukiasyan, S. Patchkovskii, O. Smirnova, T. Brabec, and M. Y. Ivanov, Phys. Rev. A **82**, 043414 (2010).
[11] T. Morishita, A.-T. Le, Z. Chen, and C. D. Lin, Phys. Rev. Lett. **100**, 013903 (2008).
[12] C. Lin, A.-T. Le, Z. Chen, T. Morishita, and R. Lucchese, J. Phys. B **43**, 122001 (2010).
[13] V. Serbinenko and O. Smirnova, J. Phys. B **46**, 171001 (2013).
[14] D. Shafir, H. Soifer, B. D. Bruner, M. Dagan, Y. Mairesse, S. Patchkovskii, M. Y. Ivanov, O. Smirnova, and N. Dudovich, Nature (London) **485**, 343 (2012).
[15] D. Shafir, Y. Mairesse, H. Wörner, K. Rupnik, D. Villeneuve, P. Corkum, and N. Dudovich, New J. Phys. **12**, 073032 (2010).
[16] S. Ghimire, A. D. DiChiara, E. Sistrunk, P. Agostini, L. F. DiMauro, and D. A. Reis, Nature Phys. **7**, 138 (2011).
[17] O. Schubert, M. Hohenleutner, F. Langer, B. Urbanek, C. Lange, U. Huttner, D. Golde, T. Meier, M. Kira, S. W. Koch, and R. Huber, Nature Photon. **8**, 119 (2014).
[18] S. Ghimire, A. D. DiChiara, E. Sistrunk, G. Ndabashimiye, U. B. Szafruga, A. Mohammad, P. Agostini, L. F. DiMauro, and D. A. Reis, Phys. Rev. A **85**, 043836 (2012).
[19] O. D. Mücke, Phys. Rev. B **84**, 081202 (2011).
[20] D. Golde, T. Meier, and S. W. Koch, Phys. Rev. B **77**, 075330 (2008).
[21] P. G. Hawkins and M. Y. Ivanov, Phys. Rev. A **87**, 063842 (2013).
[22] G. Vampa, C. R. McDonald, G. Orlando, D. D. Klug, P. B. Corkum, and T. Brabec, Phys. Rev. Lett. **113**, 073901 (2014).
[23] T. Higuchi, M. I. Stockman, and P. Hommelhoff, Phys. Rev. Lett. **113**, 213901 (2014).
[24] L. Plaja and L. Roso-Franco, Phys. Rev. B **45**, 8334 (1992).
[25] J. B. Krieger and G. J. Iafrate, Phys. Rev. B **33**, 5494 (1986).
[26] R. Resta, J. Phys.: Condens Matter **12**, R107 (2000).